

On the Distance of SGR 1935+2154 Associated with FRB 200428

SHU-QING ZHONG,^{1,2} ZI-GAO DAI,^{1,2} HAI-MING ZHANG,^{1,2} AND CAN-MIN DENG^{3,4}

¹*School of Astronomy and Space Science, Nanjing University, Nanjing 210093, China; dzg@nju.edu.cn*

²*Key laboratory of Modern Astronomy and Astrophysics (Nanjing University), Ministry of Education, Nanjing 210093, China*

³*Department of Astronomy, School of Physical Sciences, University of Science and Technology of China, Hefei, Anhui 230026, China*

⁴*CAS Key Laboratory for Research in Galaxies and Cosmology, Department of Astronomy, University of Science and Technology of China, Hefei 230026, Anhui, China*

ABSTRACT

Owing to the detection of an extremely bright fast radio burst (FRB) 200428 from SGR 1935+2154 associated with a hard X-ray counterpart, the distance of SGR 1935+2154 potentially hosted in the supernova remnant (SNR) G57.2+0.8 can be revisited. Under the assumption that the SGR and the SNR are realistically related, in this Letter, we investigate the dispersion measure (DM) of this radio burst contributed by the foreground medium of our Galaxy and the local environments including a magnetar wind nebula and SNR, and by combining the current observational results about the SGR and SNR, we find that the distance is in a narrow range of 9.06 to 9.11 kpc and the SNR radius falls into 14.5–14.6 pc since the local DM contribution is as low as 0–5 pc cm⁻³. These results are basically consistent with the previous studies but appear to be more constrained. Additionally, the study for the Faraday rotation measure of the SGR and SNR is also available.

Keywords: Magnetars (992); Soft gamma-ray repeaters (1471); Radio transient sources (2008)

1. INTRODUCTION

Very recently, an extremely bright millisecond-timescale radio burst from the direction of the Galactic magnetar SGR 1935+2154 was reported by The CHIME/FRB Collaboration et al. (2020) and Bochenek et al. (2020). More excitingly, its potentially associated X-ray counterpart was also detected by Insight-HXMT (Zhang et al. 2020b,c,d), AGILE (Tavani et al. 2020), INTEGRAL (Mereghetti et al. 2020), and Konus-Wind (Ridnaia et al. 2020) telescopes. In addition, a subsequent highly polarised radio burst with Faraday rotation measure (RM) +112.3 rad m⁻² was detected by the FAST radio telescope (Zhang et al. 2020a), approximately consistent with RM = +116 ± 2 ± 5 rad m⁻² of FRB 200428 (The CHIME/FRB Collaboration et al. 2020). From the previous investigations about the magnetar SGR 1935+2154, it has a spin period $P \simeq 3.24$ s, a spin-down rate $\dot{P} \simeq 1.43 \times 10^{-11}$ ss⁻¹, a surface dipole magnetic field strength $B_p \simeq 2.2 \times 10^{14}$ G, an age $t \sim 3.6$ kyr, and a spin-down luminosity $L_{sd} \sim 1.7 \times 10^{34}$ erg s⁻¹ (Israel et al. 2016), possibly hosted in the Galactic supernova remnant (SNR) G57.2+0.8 (Gaensler 2014).

In the literature, however, the distance of SNR G57.2+0.8 has a large range and remains highly debated even though many authors have used various

methods, e.g., the statistical radio surface-brightness-to-diameter relation (~ 9.1 kpc; Pavlović et al. 2013), the empirical relation between the hydrogen column density N_H and the dispersion measure (DM) (11.7±2.8 kpc; Surnis et al. 2016), and the local standard of rest (LSR) velocity measure via HI absorption feature (12.5±1.5 kpc; Kothes et al. 2018), (4.5-9.0 kpc; Ranasinghe et al. 2018), and CO gas towards the SNR (6.6±0.7 kpc; Zhou et al. 2020). For SGR 1935+2154, Kozlova et al. (2016) gave an upper limit < 10 kpc through the scattered link between the squares of the radii of the emitting areas and their black-body temperatures.

In this Letter, we assume SGR 1935+2154 is indeed associated with both SNR G57.2+0.8 and FRB 200428 and the SNR has the same age with SGR 1935+2154, and then purely use the DM and combine with current observations to estimate the distance in Section 2. Our results are displayed in Section 3. A discussion on RM estimate and results is arranged in Section 4, and conclusions are drawn in Section 5.

2. DM ESTIMATE

Based on the observations of CHIME and STARES radio telescopes, The CHIME/FRB Collaboration et al. (2020) and Bochenek et al. (2020) reported that the FRB from SGR 1935+2154 has analogous DM_{obs} =

$332.7206 \pm 0.0009 \text{ pc cm}^{-3}$ and $332.702 \pm 0.008 \text{ pc cm}^{-3}$, respectively. The observed DM_{obs} is mainly contributed by the foreground interstellar medium (ISM) in our Galaxy (DM_{Gal}), the magnetar wind nebula (DM_{MWN}), and the SNR (DM_{SNR}), that is,

$$\text{DM}_{\text{obs}} = \text{DM}_{\text{Gal}} + \text{DM}_{\text{MWN}} + \text{DM}_{\text{SNR}}, \quad (1)$$

where the foreground DM of our Galaxy

$$\text{DM}_{\text{Gal}} = \int_0^D n_e(l) dl, \quad (2)$$

which is related to the distance D of SGR 1935+2154 that can be obtained via the Galactic electron density (n_e) model NE2001 (Cordes & Lazio 2002) (or YMW16; Yao et al. 2017).

The DM_{MWN} is principally attributed to O-mode wave and may be given by (e.g., Yu 2014; Cao et al. 2017; Yang & Zhang 2017)

$$\text{DM}_{\text{MWN}} \simeq 0.082 \text{ pc cm}^{-3} \mu_{\pm,4}^{2/3} B_{\text{p},14}^{4/3} P_0^{-11/3}, \quad (3)$$

where $\mu_{\pm} = 10^4 \mu_{\pm,4}$ is the multiplicity parameter of the electron-positron pairs, $B_{\text{p}} = 10^{14} B_{\text{p},14} \text{ G}$ is the dipole magnetic field, and $P = 10^0 P_0 \text{ s}$ is the rotation period of the magnetar.

In regard to the DM_{SNR} , it heavily depends on the ambient medium: constant density ISM or wind environment. So we consider the DM contribution by the SNR in two different scenarios as follows.

2.1. Constant ISM

It is widely believed that an SNR has three phases after a supernova (SN) explosion in the constant ISM scenario: (a) the free-expansion phase, (b) the Sedov-Taylor phase, (c) and the snowplow phase. Since SNR G57.2+0.8 has possibly reached the end of the Sedov-Taylor phase or entered the snowplow phase due to the non-detection of X-ray emission (Kothes et al. 2018; Zhou et al. 2020), the DM_{SNR} for the ionized medium (including shocked ejecta and shocked swept ambient medium¹), can be estimated by

$$\text{DM}_{\text{SNR}} \simeq \begin{cases} 34 \text{ pc cm}^{-3} t_2^{2/5} E_{51}^{1/5} n_2^{4/5}, & t < t_{\text{SP}} \\ 81 \text{ pc cm}^{-3} t_3^{2/7} E_{51}^{0.225} n_2^{0.737}, & t > t_{\text{SP}} \end{cases} \quad (4)$$

during the Sedov-Taylor and snowplow phases (e.g., Yang & Zhang 2017; Piro & Gaensler 2018), where $E =$

$10^{51} E_{51} \text{ erg}$ is the energy of the explosion, $t_i = t/10^i \text{ yr}$, and $n = 10^2 n_2 \text{ cm}^{-3}$ is the number density of a uniform ambient ISM, as well as the snowplow time $t_{\text{SP}} \simeq 3920 \text{ yr } E_{51}^{0.22} n_2^{-0.55}$ (e.g., Draine 2011). The corresponding SNR radius during different phases can be written by (e.g., Taylor 1950; Sedov 1959; Draine 2011; Yang & Zhang 2017)

$$R_{\text{SNR}} \simeq \begin{cases} 0.84 \text{ pc } t_2^{2/5} E_{51}^{1/5} n_2^{-1/5}, & t < t_{\text{SP}} \\ 2.44 \text{ pc } t_3^{2/7} E_{51}^{0.225} n_2^{-0.263}, & t > t_{\text{SP}} \end{cases} \quad (5)$$

Here we use the Sedov-Taylor radius independent of the SN ejecta mass as the SNR radius (Yang & Zhang 2017) rather than the blastwave radius depending on the SN ejecta mass (Piro & Gaensler 2018) can be a good approximation when the SNR probably has reached the end of the Sedov-Taylor phase or entered the snowplow phase.

2.2. Wind Environment

In the wind scenario, the SNR evolution has two phases: the early ejecta-dominated phase and the wind-dominated phase occurring at very late times, based on Piro & Gaensler (2018). During different phases, the DM_{SNR} is calculated by (see Table 2 of Piro & Gaensler 2018)

$$\text{DM}_{\text{SNR}} \simeq \begin{cases} 13 \text{ pc cm}^{-3} \mu_e^{-1} t_2^{-3/2} E_{51}^{-3/4} M_1^{5/4} K_{13}^{1/2}, & t < t_{\text{ch}} \\ 0.088 \text{ pc cm}^{-3} \mu_e^{-1} t_3^{-2/3} E_{51}^{-1/3} K_{13}^{4/3}, & t > t_{\text{ch}} \end{cases} \quad (6)$$

where μ_e is the mean molecular weight per electron, $M = M_1 \times 1 M_{\odot}$ is the mass of the SN ejecta, $K = 5.1 \times 10^{13} \text{ g cm}^{-1} \dot{M}_{-5} v_6^{-1}$ (here, the mass-loss rate $\dot{M}_{-5} = 10^{-5} M_{\odot} \text{ yr}^{-1}$ and the wind velocity $v_6 = v_w/10^6 \text{ cm s}^{-1}$), and the characteristic time $t_{\text{ch}} = 1.9 \times 10^3 \text{ yr } E_{51}^{-1/2} M_1^{3/2} K_{13}^{-1}$ separating the two phases. This characteristic time corresponds to a radius $R_{\text{ch}} = 16.8 \text{ pc } M_1 K_{13}^{-1}$. Such that the SNR radius regarded as the blastwave radius can be related to R_{ch} and t_{ch} through the analytic functions (see Table 2 of Piro & Gaensler 2018)

$$R_{\text{SNR}} \simeq \begin{cases} 1.79 R_{\text{ch}} (t/t_{\text{ch}}) \left[1 + 0.33 (t/t_{\text{ch}})^{1/2} \right]^{-2}, & t < t_{\text{ch}} \\ [1.11 (t/t_{\text{ch}}) - 0.11]^{2/3} R_{\text{ch}}, & t > t_{\text{ch}} \end{cases} \quad (7)$$

¹ We assume the swept ambient medium is fully ionized and also neglect the unshocked ambient medium in the upstream of the shock since it is neutral hydrogen dominated.

3. DM RESULTS

A very useful observational constraint for SNR G57.2+0.8 is that it is an almost circular source with an average diameter about $10'$, i.e., radius $\theta_r \approx 5'.5$ (Kothés et al. 2018), which relates to the SNR radius via the distance D

$$D = \frac{R_{\text{SNR}}}{\theta_r}. \quad (8)$$

In addition, the observational constraints for DM_{obs} , t , B_p , and P are also known. Through the calculations of Equation (3), we can find that the value of DM_{MWN} is far smaller than 1 pc cm^{-3} even if μ_{\pm} is very large like 10^6 , so we safely ignore this term in Equation (1) for subsequent calculations.

In the ISM scenario for the SNR, combining Equations (1), (2)², (4), (5), and (8), we can get a power-law relation with an index 1.0 between the explosion energy E and the ambient medium density n , as illustrated in the top panel of Figure 1. It also shows that the ambient medium density favors a relatively low value $< 1 \text{ cm}^{-3}$. Meanwhile, we can also acquire a narrow distance distribution $D \simeq 9.06 - 9.11 \text{ kpc}$, a narrow SNR radius $R_{\text{SNR}} \simeq 14.5 - 14.6 \text{ pc}$, and a limited $\text{DM}_{\text{SNR}} \simeq 0 - 5 \text{ pc cm}^{-3}$ illustrating in the middle and bottom panel of Figure 1, within a typical SN explosion energy ranging from a few 10^{49} erg to several 10^{51} erg (e.g., Pejcha & Prieto 2015; Lyman et al. 2016). Visibly, it can also be seen that the DM_{SNR} is very low at the current age $t = 3.6 \text{ kyr}$ of SGR 1935+2154, compared to the Galactic contribution DM_{Gal} .

For the wind environment towards the SNR, employing Equations (1), (2), (6)³, (7), and (8), we obtain a relation between the explosion energy E and the parameter K for $M = 2 M_{\odot}$ (stripped-envelope SNe) and $M = 10 M_{\odot}$ (red supergiant progenitors), as appeared in Figure 2. The parameter K declines sharply when the explosion energy $E < 4 \times 10^{50} \text{ erg}$ ($E < 2 \times 10^{51} \text{ erg}$) for $M = 2 M_{\odot}$ ($M = 10 M_{\odot}$), so we estimate the evolutions of other parameters by only considering the explosion energy $E > 4 \times 10^{50} \text{ erg}$ ($E > 2 \times 10^{51} \text{ erg}$) for $M = 2 M_{\odot}$ ($M = 10 M_{\odot}$). Other panels of Figure 2 exhibit that the distance spans $D \simeq 9.06 - 9.11 \text{ kpc}$ and the DM contribution of the SNR occupies $\text{DM}_{\text{SNR}} \simeq 0 - 5 \text{ pc cm}^{-3}$ for different SN ejecta mass. These results are in comparison with those in ISM scenario.

In summary, our results seem more compact even though they are generally consistent with those in previous studies by Pavlović et al. (2013), Surnis et al.

(2016), Kothés et al. (2018), Ranasinghe et al. (2018), and Zhou et al. (2020) for SNR G57.2+0.8, and Kozlova et al. (2016) for SGR 1935+2154. The former methods in Pavlović et al. (2013), Surnis et al. (2016), and Kozlova et al. (2016) are empirical and statistical, with intrinsic large scatter. The latter seem to be more direct methods and they are mainly related to the uncertainties of the LSR velocity measure and the rotation curve of the Galaxy. In contrast, the distance estimate from DM in this paper is assumption-dependent and model-dependent but the results seem to be not significantly changeable in different models. The uncertainty in this method maybe mainly originate from the Galactic electron density distribution of YMW16 model.

4. RM ESTIMATE

Similarly to the DM estimate, the observed RM_{obs} should also has three parts: the foreground RM_{Gal} due to the Galactic ISM and permeating magnetic fields, the RM_{MWN} contributed by the magnetic wind nebula, and the RM_{SNR} resulted from the SNR, read as

$$\text{RM}_{\text{obs}} = \text{RM}_{\text{Gal}} + \text{RM}_{\text{MWN}} + \text{RM}_{\text{SNR}}. \quad (9)$$

(1) The first part RM_{Gal} can be expressed as

$$\text{RM}_{\text{Gal}}[\text{rad m}^{-2}] = 0.81 \int_0^D n_e[\text{cm}^{-3}] B_{\parallel}[\mu\text{G}] dl[\text{pc}] \quad (10)$$

where B_{\parallel} is the component of the Galactic magnetic field (GMF) parallel to the line of sight. RM is positive when the magnetic field points towards us. There is a general model of the GMF consisting of two different components: a disk field and a halo field (Prouza & Šmída 2003; Sun et al. 2008). The widely used disk field is the logarithmic spiral disk GMF model, which has two versions: the axisymmetric disk field (ASS model) and the bisymmetric disk field (BSS model) (e.g., Simard-Normandin & Kronberg 1980; Han & Qiao 1994; Stanev 1997; Tinyakov & Tkachev 2002). To estimate the RM_{Gal} , we consider the disk field with an ASS form or BSS form and halo field with a basic form (Prouza & Šmída 2003; Sun et al. 2008; Jansson et al. 2009; Sun & Reich 2010; Pshirkov et al. 2011) as done in Lin & Dai (2016), combining with the Galactic free electron distribution n_e in Yao et al. (2017) and the distance $D \simeq 9 \text{ kpc}$ from DM estimate. However, the RM_{Gal} has different values in different models or in same models but with different parameters, from a few tens to several hundreds of rad m^{-2} , e.g., $\sim 670 \text{ rad m}^{-2}$ for ASS+halo and $\sim 270 \text{ rad m}^{-2}$ for BSS+halo in Pshirkov et al. (2011), and -82 rad m^{-2} for ASS+halo in Sun et al. (2008). Therefore, it cannot be well estimated by the GMF models. Otherwise, Kothés et al.

² Here, we adopt the YMW16 model whose code has been built-in the pyymw16 package of Python.

³ We adopt $\mu_e = 1$. The values of μ_e in a reasonable range cannot significantly influence the final results.

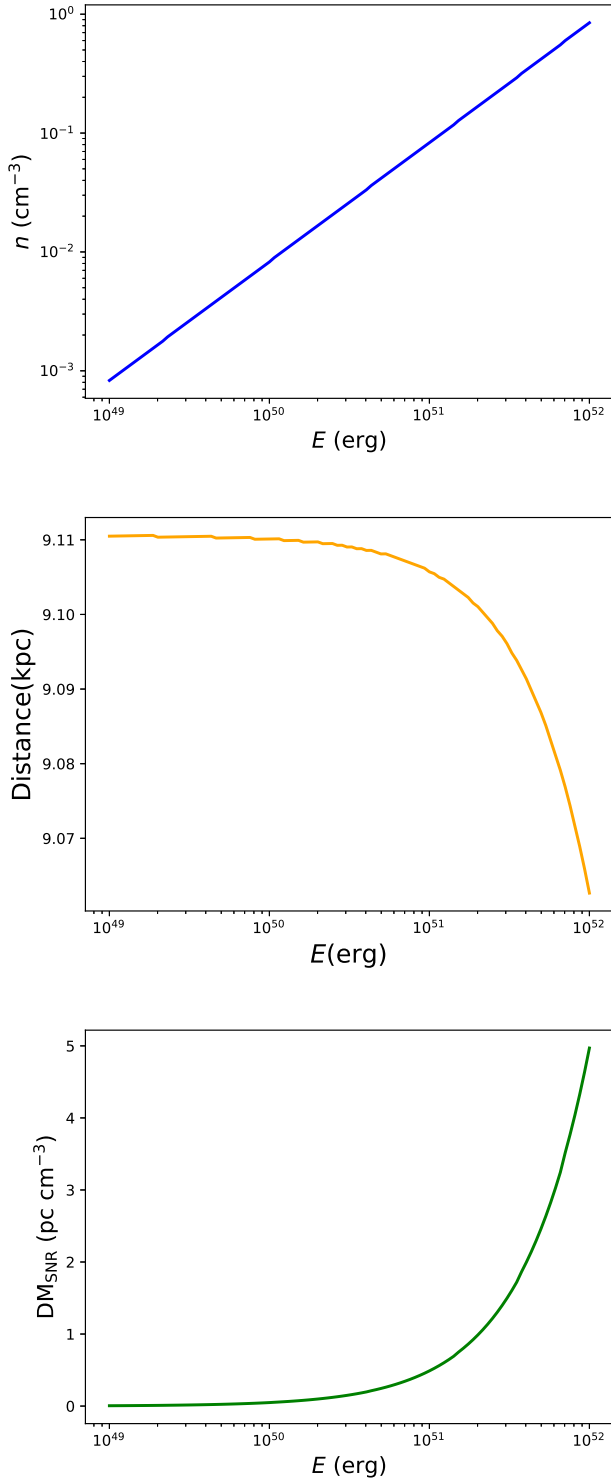


Figure 1. In the constant ISM for the SNR: (a) ambient medium density n as a power-law function of SN explosion energy E (top panel); (b) the distance D of SGR 1935+2154 evolves with the SN explosion energy E (middle panel); (c) the DM_{SNR} contributed by the SNR is relevant to the SN explosion energy E (bottom panel).

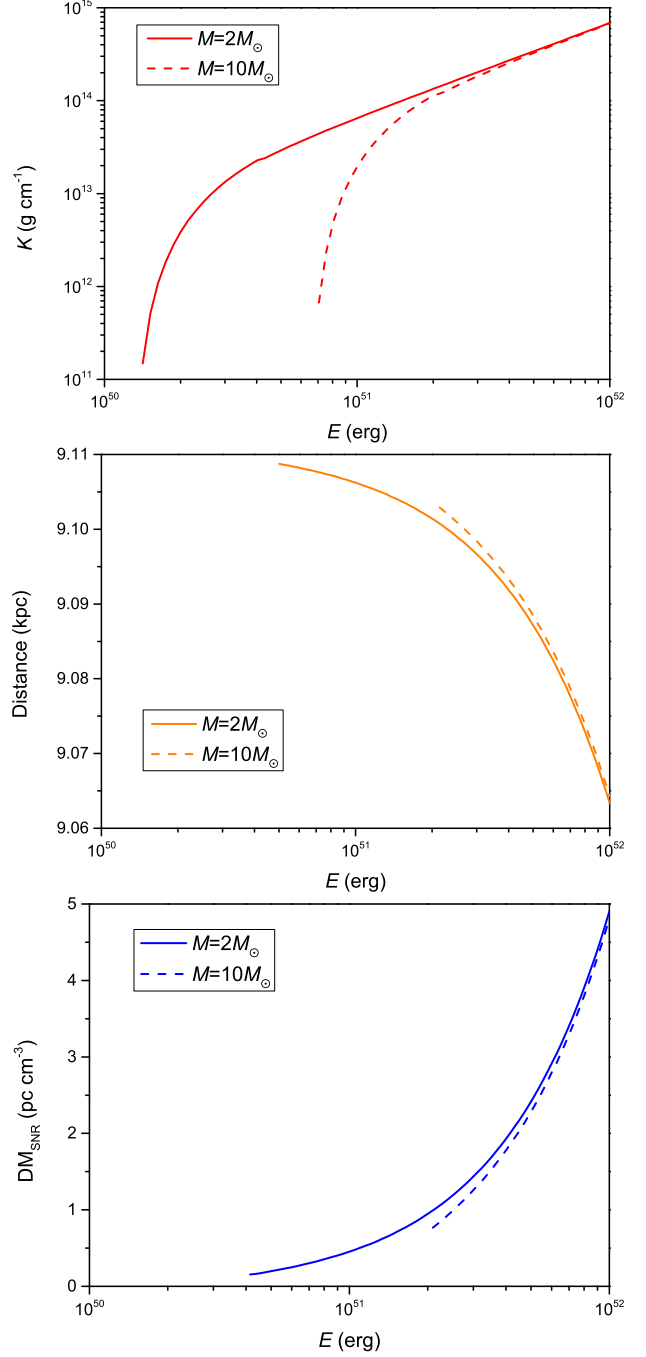


Figure 2. In the wind environment for the SNR: (a) the parameter $K = 5.1 \times 10^{13} \text{ g cm}^{-1} \dot{M}_{-5} v_6^{-1}$ as a function of explosion energy E of supernova (top panel); (b) same as the middle panel of Figure 1 (middle panel); (c) same as the bottom panel of Figure 1 (bottom panel).

(2018) found that the foreground $RM = +223 \pm 2 \text{ rad m}^{-2}$ for SNR G57.2+0.8 via the polarized intensity maps.

(2) The second part RM_{MWN} is primarily caused by the magnetar wind nebula due to the magnetar spin-

down energy release. The magnetic field of the nebula at time t can be crudely estimated by (Metzger et al. 2017)

$$B_n \simeq \left(\frac{6\epsilon_B L_{sd} t}{R_n^3} \right)^{1/2}, \quad (11)$$

where ϵ_B is the ratio of the magnetic energy to the shock energy. Assuming $R_n \sim (0.01 - 0.1)R_{SNR} \simeq 0.1 - 1$ pc (R_{SNR} is gained in section 3), and giving $\epsilon_B \sim 0.1$, $L_{sd} \sim 1.7 \times 10^{34}$ erg s $^{-1}$, and $t \sim 3.6$ kyr, one would get $B_n \sim 1 - 100 \mu\text{G}$. In this case, a very low $\text{RM}_{\text{MWN}} \simeq 0.81 \text{ rad m}^{-2} \frac{\text{DM}_{\text{MWN}}}{\text{pc cm}^{-3}} \frac{B_n}{\mu\text{G}} \sim 0.01 - 0.3 \text{ rad m}^{-2}$ is acquired through Equation (3). Even though some parameters are uncertain, the RM_{MWN} should be low if they locate in reasonable ranges.

(3) Akin to DM_{SNR} estimate, RM_{SNR} in different surrounding environments also has distinct evolutions.

ISM Scenario. In the snowplow phase, SNR velocity reads (Yang & Zhang 2017)

$$v_{\text{SP}} = 690 \text{ km s}^{-1} t_3^{-5/7} E_{51}^{0.445} n_2^{-0.813}. \quad (12)$$

So that the magnetic field generated in the shocked ISM is estimated as (Piro & Gaensler 2018)

$$\begin{aligned} B_{\text{ISM}} &\approx (16\pi\epsilon m_p n)^{1/2} v_{\text{SP}} \\ &\approx 2.02 \times 10^3 \mu\text{G} \epsilon_{-1}^{1/2} t_3^{-5/7} E_{51}^{0.445} n_2^{-0.313} \end{aligned} \quad (13)$$

where $\epsilon = 10^{-1}\epsilon_{-1}$ is the ratio of the magnetic energy to the shock energy. Hence, the RM_{SNR} in the snowplow phase ($t > t_{\text{SP}}$) deduced from Equations (4) and (13) can be written down as, along with the RM_{SNR} in the Sedov-Taylor phase ($t < t_{\text{SP}}$) (Piro & Gaensler 2018),

$$\text{RM}_{\text{SNR}} \simeq \begin{cases} 1.28 \times 10^5 \text{ rad m}^{-2} \epsilon_{-1}^{1/2} t_3^{-1/5} E_{51}^{2/5} n_2^{11/10}, & t < t_{\text{SP}} \\ 4.94 \times 10^4 \text{ rad m}^{-2} \epsilon_{-1}^{1/2} t_4^{-3/7} E_{51}^{0.67} n_2^{0.424}, & t > t_{\text{SP}} \end{cases} \quad (14)$$

Combining with the result between the energy of explosion E and the number density n of ambient ISM in the top panel of Figure 1, one can derive RM_{SNR} as a power-law function of the explosion energy with an index 1.5, as displayed in the left panel of Figure 3. It is shown that RM_{SNR} can increase up to 10^3 rad m^{-2} when E approaches to 10^{52} erg.

Wind Scenario. The RM_{SNR} in wind environment is calculated by (Piro & Gaensler 2018)

$$\text{RM}_{\text{SNR}} \simeq \begin{cases} 0.002 \text{ rad m}^{-2} x_{0.1} R_{*,2} B_{*,0} \mu_e^{-1} E_{51}^{-1} M_1 t_3^{-2}, & t < t_{\text{ch}} \\ 0.0017 \text{ rad m}^{-2} x_{0.1} R_{*,2} B_{*,0} \mu_e^{-1} E_{51}^{-2/3} K_{13}^{5/3} t_4^{-4/3} \text{pllosion energy } E \sim 2 \times 10^{51} \text{ erg in ISM scenario from left panel of Figure 3.} \end{cases} \quad (15)$$

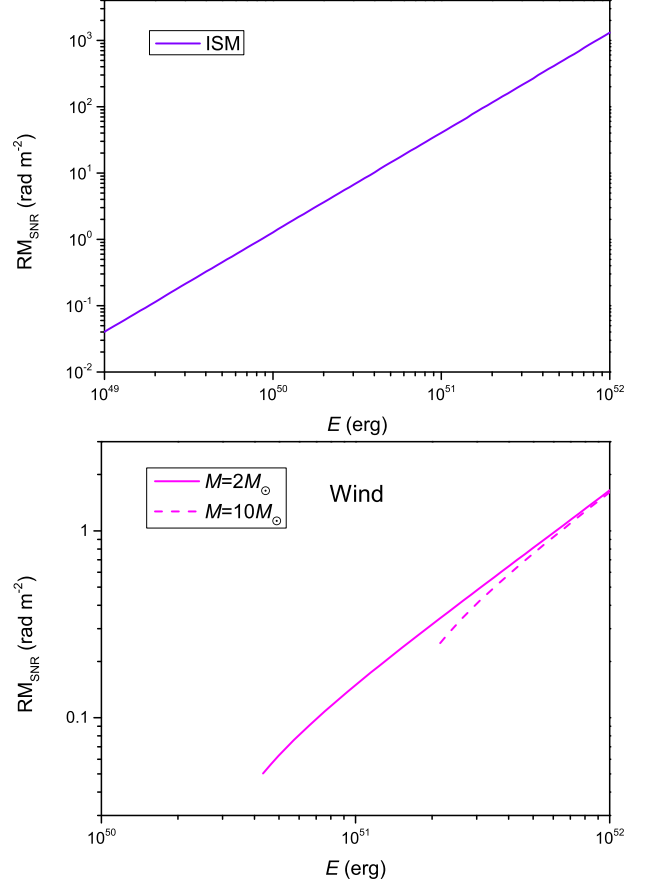


Figure 3. The RM_{SNR} vs. the energy of explosion E in ISM (left panel) and wind (right panel) environments.

where $x \equiv v_{\text{rot}}/v_w$ (v_{rot} and v_w are the rotation velocity and wind velocity), $R_* = 100 R_\odot R_{*,2}$ and $B_* = 10^0 B_{*,0}$ G are the progenitor's radius and magnetic field, respectively. Fixing $x = 0.1$, $R_* = 100 R_\odot$, $\mu_e = 1$, and $B_* = 1$ G (even if they should be variable for different types of progenitors), and utilizing the relation between the energy of explosion E and the parameter K in the top panel of Figure 2 for different progenitors ($M = 2M_\odot$ and $M = 10M_\odot$), one gains a low $\text{RM}_{\text{SNR}} < 2 \text{ rad m}^{-2}$ in the explosion energy $E < 10^{52}$ erg, as in the right panel of Figure 3.

As we can see, the foreground $\text{RM} = +223 \pm 2 \text{ rad m}^{-2}$ for SNR G57.2+0.8 (Kothes et al. 2018), a highly polarised radio burst with $\text{RM}_{\text{obs}} = +112.3 \text{ rad m}^{-2}$ for SGR 1935+2154 (Zhang et al. 2020a). If SGR 1935+2154 and SNR G57.2+0.8 is actually related to each other and the foreground RM is not contributed by the local environment of the SNR, it could indicate the $\text{RM}_{\text{SNR}} \sim -110 \text{ rad m}^{-2}$, suggesting a possible explosion energy $E \sim 2 \times 10^{51}$ erg in ISM scenario from left panel of Figure 3.

5. CONCLUSIONS

In this paper, we have purely utilized DM contributed by the foreground ISM of our Galaxy and the local environments including the magnetar wind nebula and SNR to estimate the distance of SGR 1935+2154 and SNR G57.2+0.8, assuming the SGR and SNR are realistically related and combining with other certain observations. Moreover, RM estimate and results have been also discussed. Some interesting results are as follows:

- In the constant ISM scenario for the SNR, the SN explosion energy E has a power-law function as the ambient medium density n with a positive index. Moreover, the distance, SNR radius, and DM contributed by the SNR narrowly distribute $D \simeq 9.06 - 9.11$ kpc, $R_{\text{SNR}} \simeq 14.5 - 14.6$ pc, and $\text{DM}_{\text{SNR}} \simeq 0 - 5$ pc cm $^{-3}$ in a typical region of the explosion energy, respectively.
- In the wind scenario for the SNR, the distance, SNR radius and DM_{SNR} also spread over similar ranges of those in the ISM scenario for different SN ejecta mass. But the acceptable explosion energy is more confined.
- For the RM estimate, the polarization observations from the radio burst of the SGR and the intensity maps of the SNR might signify the RM contribution by the local environment of the SNR is about -110 rad m $^{-2}$, which corresponds to the explosion energy $\sim 2 \times 10^{51}$ erg.

On the whole, our results relevant to DM are basically consistent with the previous studies but tighter than them.

ACKNOWLEDGMENTS

We would like to thank Wei-Li Lin for her helpful discussions. This work was supported by the National Key Research and Development Program of China (grant No. 2017YFA0402600) and the National Natural Science Foundation of China (grant No. 11833003). C.M.D. is partially supported by the Fundamental Research Funds for the Central Universities (NO. WK2030000019).

REFERENCES

- Bochenek, C. D., Ravi, V., Belov, K. V., et al. 2020, arXiv e-prints, arXiv:2005.10828.
<https://arxiv.org/abs/2005.10828>
- Cao, X.-F., Yu, Y.-W., & Dai, Z.-G. 2017, ApJL, 839, L20, doi: [10.3847/2041-8213/aa6af2](https://doi.org/10.3847/2041-8213/aa6af2)
- Cordes, J. M., & Lazio, T. J. W. 2002, arXiv e-prints, astro. <https://arxiv.org/abs/astro-ph/0207156>
- Draine, B. T. 2011, Physics of the Interstellar and Intergalactic Medium (Princeton, NJ: Princeton Univ. Press)
- Gaensler, B. M. 2014, GRB Coordinates Network, 16533, 1
- Han, J. L., & Qiao, G. J. 1994, A&A, 288, 759
- Israel, G. L., Esposito, P., Rea, N., et al. 2016, MNRAS, 457, 3448, doi: [10.1093/mnras/stw008](https://doi.org/10.1093/mnras/stw008)
- Jansson, R., Farrar, G. R., Waelkens, A. H., & Enßlin, T. A. 2009, JCAP, 2009, 021, doi: [10.1088/1475-7516/2009/07/021](https://doi.org/10.1088/1475-7516/2009/07/021)
- Kothes, R., Sun, X., Gaensler, B., & Reich, W. 2018, ApJ, 852, 54, doi: [10.3847/1538-4357/aa9e89](https://doi.org/10.3847/1538-4357/aa9e89)
- Kozlova, A. V., Israel, G. L., Svinkin, D. S., et al. 2016, MNRAS, 460, 2008, doi: [10.1093/mnras/stw1109](https://doi.org/10.1093/mnras/stw1109)
- Lin, W.-L., & Dai, Z.-G. 2016, Research in Astronomy and Astrophysics, 16, 38, doi: [10.1088/1674-4527/16/3/038](https://doi.org/10.1088/1674-4527/16/3/038)
- Lyman, J. D., Bersier, D., James, P. A., et al. 2016, MNRAS, 457, 328, doi: [10.1093/mnras/stv2983](https://doi.org/10.1093/mnras/stv2983)
- Mereghetti, S., Savchenko, V., Ferrigno, C., et al. 2020, arXiv e-prints, arXiv:2005.06335.
<https://arxiv.org/abs/2005.06335>
- Metzger, B. D., Berger, E., & Margalit, B. 2017, ApJ, 841, 14, doi: [10.3847/1538-4357/aa633d](https://doi.org/10.3847/1538-4357/aa633d)
- Pavlović, M. Z., Urošević, D., Vukotić, B., Arbutina, B., & Göker, Ü. D. 2013, ApJS, 204, 4, doi: [10.1088/0067-0049/204/1/4](https://doi.org/10.1088/0067-0049/204/1/4)
- Pejcha, O., & Prieto, J. L. 2015, ApJ, 806, 225, doi: [10.1088/0004-637X/806/2/225](https://doi.org/10.1088/0004-637X/806/2/225)
- Piro, A. L., & Gaensler, B. M. 2018, ApJ, 861, 150, doi: [10.3847/1538-4357/aac9bc](https://doi.org/10.3847/1538-4357/aac9bc)
- Prouza, M., & Šmída, R. 2003, A&A, 410, 1, doi: [10.1051/0004-6361:20031281](https://doi.org/10.1051/0004-6361:20031281)
- Pshirkov, M. S., Tinyakov, P. G., Kronberg, P. P., & Newton-McGee, K. J. 2011, ApJ, 738, 192, doi: [10.1088/0004-637X/738/2/192](https://doi.org/10.1088/0004-637X/738/2/192)
- Ranasinghe, S., Leahy, D. A., & Tian, W. 2018, Open Physics Journal, 4, 1, doi: [10.2174/1874843001804010001](https://doi.org/10.2174/1874843001804010001)
- Ridnaia, A., Golenetskii, S., Aptekar, R., et al. 2020, The Astronomer's Telegram, 13688, 1
- Sedov, L. I. 1959, Similarity and Dimensional Methods in Mechanics (New York: Academic Press)
- Simard-Normandin, M., & Kronberg, P. P. 1980, ApJ, 242, 74, doi: [10.1086/158445](https://doi.org/10.1086/158445)

- Stanev, T. 1997, ApJ, 479, 290, doi: [10.1086/303866](https://doi.org/10.1086/303866)
- Sun, X.-H., & Reich, W. 2010, Research in Astronomy and Astrophysics, 10, 1287, doi: [10.1088/1674-4527/10/12/009](https://doi.org/10.1088/1674-4527/10/12/009)
- Sun, X. H., Reich, W., Waelkens, A., & Enßlin, T. A. 2008, A&A, 477, 573, doi: [10.1051/0004-6361:20078671](https://doi.org/10.1051/0004-6361:20078671)
- Surnis, M. P., Joshi, B. C., Maan, Y., et al. 2016, ApJ, 826, 184, doi: [10.3847/0004-637X/826/2/184](https://doi.org/10.3847/0004-637X/826/2/184)
- Tavani, M., Ursi, A., Verrecchia, F., et al. 2020, The Astronomer’s Telegram, 13686, 1
- Taylor, G. 1950, Proceedings of the Royal Society of London Series A, 201, 159, doi: [10.1098/rspa.1950.0049](https://doi.org/10.1098/rspa.1950.0049)
- The CHIME/FRB Collaboration, :, Andersen, B. C., et al. 2020, arXiv e-prints, arXiv:2005.10324. <https://arxiv.org/abs/2005.10324>
- Tinyakov, P. G., & Tkachev, I. I. 2002, Astroparticle Physics, 18, 165, doi: [10.1016/S0927-6505\(02\)00109-3](https://doi.org/10.1016/S0927-6505(02)00109-3)
- Yang, Y.-P., & Zhang, B. 2017, ApJ, 847, 22, doi: [10.3847/1538-4357/aa8721](https://doi.org/10.3847/1538-4357/aa8721)
- Yao, J. M., Manchester, R. N., & Wang, N. 2017, ApJ, 835, 29, doi: [10.3847/1538-4357/835/1/29](https://doi.org/10.3847/1538-4357/835/1/29)
- Yu, Y.-W. 2014, ApJ, 796, 93, doi: [10.1088/0004-637X/796/2/93](https://doi.org/10.1088/0004-637X/796/2/93)
- Zhang, C. F., Jiang, J. C., Men, Y. P., et al. 2020a, The Astronomer’s Telegram, 13699, 1
- Zhang, S. N., Tuo, Y. L., Xiong, S. L., et al. 2020b, The Astronomer’s Telegram, 13687, 1
- Zhang, S. N., Zhang, B., & Lu, W. B. 2020c, The Astronomer’s Telegram, 13692, 1
- Zhang, S. N., Xiong, S. L., Li, C. K., et al. 2020d, The Astronomer’s Telegram, 13696, 1
- Zhou, P., Zhou, X., Chen, Y., et al. 2020, arXiv e-prints, arXiv:2005.03517. <https://arxiv.org/abs/2005.03517>